Mud-Cracking Effect of Sintered Silver Layer on Quantifying Heat Transfer Behavior of SiC Devices Under Power Cycling: Voronoi Tessellation Model

Fei Qin, Shuai Zhao, Yanwei Dai, Yuankun Hu, Tong An, and Yanpeng Gong

***Abstract*— Mud-cracking of the sintered silver (Ag) layer of the SiC power module is commonly found during power cycling tests. In this article, the effect of the mud-cracking of sintered Ag on the heat transfer behaviors of SiC power module is studied based on a Voronoi tessellation model. This model is verified to be reasonable on the prediction of the equivalent thermal conductivity of sintered Ag as well as the thermal resistance of power module. The effect of the crack ratio on the equivalent thermal conductivity of sintered Ag is studied and an empirical model is proposed to predict the equivalent thermal conductivity of sintered Ag containing different mud-cracking ratios. The effect of mud-cracking ratio, chip size, sintered Ag thickness, and porosity on the thermal resistance of power module are studied. An equivalent model to study the heat transfer behaviors of the power module with mud-cracking is also developed to improve the calculation efficiency. This article establishes a new method to quantitively study the heat transfer behaviors of the power module under power cycling condition.**

***Index Terms*— Mud-cracking, porosity, power cycling, sintered Ag, Voronoi model.**

I. Introduction

SiC power modules have been increasingly adopted in the present power electronic systems due to the growing demands of integration, miniaturization, and energy conservation, especially in the high switch frequency and high-temperature applications. For the SiC power module packaging, the selection of a suitable die-attach material which can endure high temperature (>250 °C) becomes a crucial issue in the areas of electronic packaging and electronic materials in recent years. Among which, sintered Ag is currently considered to be a promising candidate because of its excellent thermal and electrical conductivity and high-temperature operating performance [1], [2].

However, during the operation time of the SiC power module, the junction temperature of the SiC chip will fluctuate in cycles, which will lead the sintered Ag layer to suffer large thermal–mechanical stresses due to the mismatch of coefficient of thermal expansion (CTE) of different packaging layers [3]. Because of the porous and brittle properties, the sintered Ag layer is prone to crack under that power cycling condition. The generation of crack in the sintered Ag layer will affect the heat dissipation characteristics of the SiC power module significantly, which will accelerate the failure of the entire power module [4], [5]. Hence, it is of great significance to quantitative study the effect of the crack of sintered Ag on the heat transfer behavior of the SiC power modules under power cycling.

The crack of sintered Ag and its effect on the thermal–mechanical reliability of the power modules have been investigated by many researchers. Hutter *et al.* [6] compared the reliability of three different die attach materials for power module packaging using active power cycling test. The results show that vertical cracks were gradually generated in the sintered Ag layer after about 570 000 cycles. Moreover, the thermal resistance was also increased when the crack occurred. Similar results were also reported by Heuck *et al.* [7]. According to the study given by Herboth *et al.* [8], the crack of the sintered Ag layer forms in the corner of die and grows toward the center region during the power cycling test. Recently, Dai *et al.* [9] and [10] and Agyakwa *et al.* [11] studied the thermal and structural characterization of sintered Ag die attachments during power cycling. The results show that vertical cracks were formed in the sintered Ag layer during the power cycling test. According to the observation by X-ray current transformer (CT), the overall morphology of these cracks is like those of "mud-crack" formed as muddy sediment dries and contracts. In addition, the authors also found that the thermal conductivity of the die attachments gradually decreases with the emerging and growth of the crack. All these investigations above show that mud-cracking is usually generated in the sintered Ag layer during the operating

Manuscript received April 15, 2022; accepted April 30, 2022. Date of publication May 26, 2022; date of current version June 24, 2022. This work was supported in part by the National Natural Science Foundation of China under Grant 11902009, in part by the Beijing Municipal Natural Science Foundation under Grant 2204074, and in part by the Scientific Research Common Program of Beijing Municipal Commission of Education under Grant KM202010005034. Recommended for publication by Associate Editor L. Codecasa upon evaluation of reviewers' comments. *(Corresponding author: Yanwei Dai.)*

Fei Qin, Yanwei Dai, Tong An, and Yanpeng Gong are with the Beijing Key Laboratory of Advanced Manufacturing Technology and the Faculty of Materials and Manufacturing, Institute of Electronics Packaging Technology and Reliability, Beijing University of Technology, Beijing 100124, China (e-mail: ywdai@bjut.edu.cn).

Shuai Zhao and Yuankun Hu are with the Faculty of Materials and Manufacturing, Institute of Electronics Packaging Technology and Reliability, Beijing University of Technology, Beijing 100124, China.

Color versions of one or more figures in this article are available at https://doi.org/10.1109/TCPMT.2022.3178226.

Digital Object Identifier 10.1109/TCPMT.2022.3178226

condition of SiC power modules. The appearance of the mud-cracking will not only affect the mechanical behavior of sintered Ag layer but also influence the heat transfer behavior of the sintered Ag as well as the entire power module. Hence, it is very necessary to quantitatively study the influence of the mud-cracking on the thermal heat transfer behavior of SiC power modules.

In fact, a lot of researchers have focused on the influence of microstructure and crack on the heat transfer characteristics of sintered Ag. Youssef *et al.* [12] presented that the thermal conductivity of sintered Ag is porosity dependent which can be predicted by the typical porous material theory. Wereszczak *et al.* [13] performed the experimental investigation on thermal conductivity of sintered Ag containing different porosity levels. Choi *et al.* [14] made an experimental investigation on the sintering silver ink. Signor *et al.* [15] performed a finite element analysis based on real 3-D microstructure of sintered Ag which shows that the thermal conductivity of sintered Ag depends mainly on pore volume fraction if morphology and distribution of pores are negligible. More recently, our group [16], [17] has reported the aging effect and crack effect on the thermal conductivity of sintered Ag in which different cracking types on the thermal conductivity of sintered Ag are discussed. However, the discussions on cracking effect are under 2-D condition which is far from the real condition. The 3-D cracking effects, such as cracking patterns and cracking density, are needed to be investigated.

The studies on the characterizations of microstructure on thermal conductivity of different porous materials are available from different backgrounds [18]–[20]. Some methods have been developed by researchers to evaluate the thermal conduction behaviors of porous materials, e.g., theoretical model based on statically assumptions [21], numerical homogenization method [22], real 3-D microstructures with micro-CT scanning, or other tested methods [23]. However, the quantitative method to evaluate the thermal conduction behaviors of porous materials with mud-cracking is still very limited in available literatures.

This article developed a Voronoi tessellation finite element model to study the mud-cracking effect on the thermal transfer behaviors of the SiC power module under power cycling condition. Toward this aim, the organization of this article is listed as follows. The problem of the mud-cracking of sintered Ag layer during power cycling test is described in Section II. In Section III, the methodology of the proposed model and computational framework are presented. In Section IV, convergence analysis of the proposed model and the power cycling simulation results are obtained. The effect of crack ratio, chip size, sintered Ag thickness, and porosity on the heat transfer behaviors of the power module is discussed in Section V. An equivalent model is also presented to increase the calculation efficiency. The conclusions are drawn in Section VI.

II. Problem Description

Fig. 1 shows the geometry structure of a typical commercial SiC power module. The entire module contains a SiC metal-oxide-semiconductor field-effect transistor (MOSFET) chip, sintered Ag layer, upper copper layer, ceramic layer, bottom layer, thermal interface layer, and baseplate. The detail geometry sizes of SiC power module are given in Table I. To characterize the effect of geometry parameters on the heat transfer behaviors of the SiC power module, various geometry sizes for SiC chip and sintered Ag layer are listed in Table I.

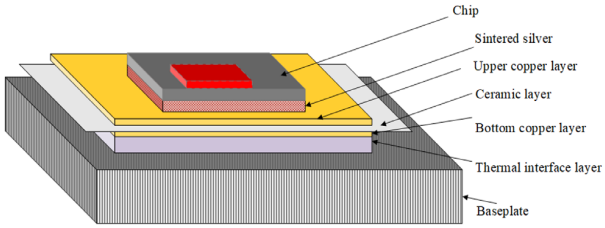

Fig. 1. Geometry structure of the typical SiC power module.

TABLE I
GEOMETRY SIZES OF THE SiC POWER MODULE

	Length (mm)	Width (mm)	Height (mm)
SiC chip	4, 6, 8, 10	4, 6, 8, 10	0.2
Sintered Ag layer	10	10	0.05, 0.1, 0.15, 0.2
Upper copper layer	30	15, 14, 9	0.3
AlN	30	40	0.38
Bottom copper layer	30	40	0.3
Thermal interface material	30	40	0.3
Baseplate	40	50	3

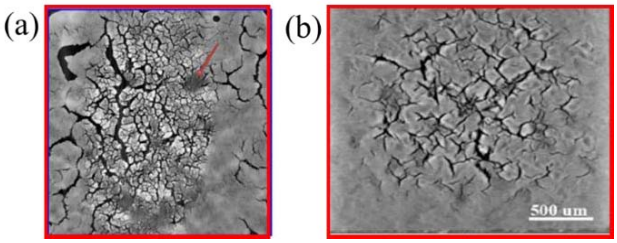

Fig. 2. Typical mud-cracking phenomenon in sintered Ag according to previous experiments. (a) Regalado *et al.* [23]. (b) Dai *et al.* [10].

As mentioned in Section I, mud-crack will appear in the sintered Ag layer during power cycling test of the SiC power module, as shown in Fig. 2. According to the experimental results performed by Regalado *et al.* [23] and Dai *et al.* [10], the crack density increases greatly with the increase of power cycles. Moreover, the appearance of crack will affect the equivalent thermal conductivity of sintered Ag layer and lead to the variation of the thermal resistance of entire power module. Hence, a quantitative model is needed to characterize the heat transfer behavior of the power module considering the mud-cracking of sintered Ag under power cycling.

III. Physical Model and Theoretical Foundation

A. Voronoi Tessellation Based Model

Voronoi is a classical method to reconstruct the microstructure of polycrystalline metal material. Common numerical procedures can be found easily in various kinds of software. Fig. 3 shows the Voronoi polygons generated by commercial software MATLAB where the black dot represents the control

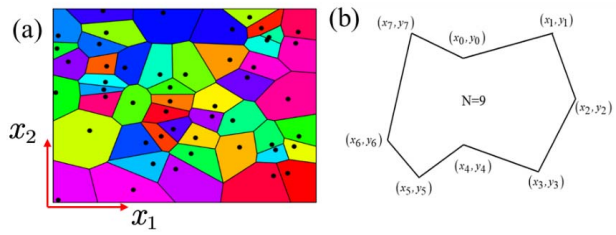

Fig. 3. Configurations of Voronoi map under 2-D condition. (a) Voronoi polygons. (b) Arbitrary polygon.

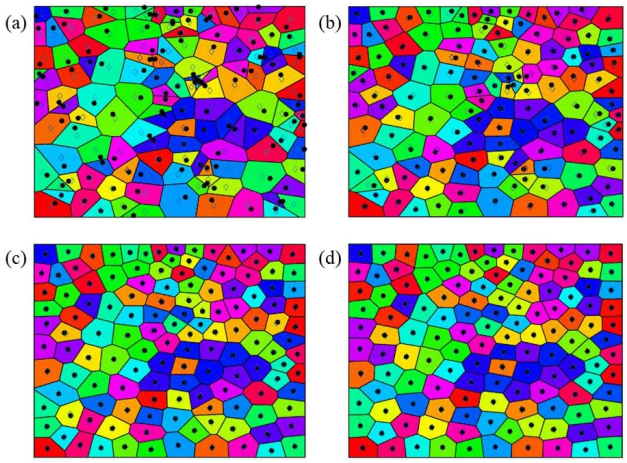

Fig. 4. Iteration scheme for generation of Voronoi polygon with iteration numbers. (a) 0. (b) 1. (c) 4. (d) 10.

point of one Voronoi polygon. One obvious shortage of the presented Voronoi polygons is that the polygons generated are very irregular, which will lead to the difficulties in grid meshing and solution. Hence, an improved Voronoi polygon generation algorithm is needed.

In order to generate homogeneously distributed Voronoi polygons, a homogeneous scheme is presented. First, the location of the mass center of every Voronoi polygon is computed, as shown in Fig. 4(a), where the hollow rhombi represents the mass center of the Voronoi polygons. Note that the primary generated control point may not coincide with the real mass center of the Voronoi polygon. Then, an iteration algorithm is started to take the mass centers of the Voronoi polygons generated at the first time as the control points of the Voronoi polygons will be generated at the next time. If the locations of the mass centers of the Voronoi polygons generated at the first time coincide well with those generated at the second time, the iteration algorithm is ended. If not, a new iteration will begin until the mass centers calculated at the nth time coincide well with those calculated at the $(n-1)$th time. Fig. 4 shows the Voronoi polygons generated after zero-, one-, four-, and ten-times iteration. It is seen that the Voronoi polygons become very regular and homogeneous after ten-times iteration.

To build the geometric model of the mud-cracking sintered Ag layer, another important problem is the generation of cracks among different polygons. In order to generate the cracks among different polygons, the following procedures

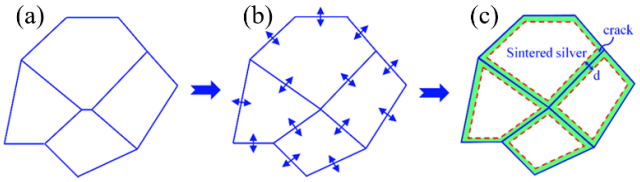

Fig. 5. Procedures to generate the mud-cracks in planar: (a) generate Voronoi polygon; (b) eliminate short side; (c) position offset.

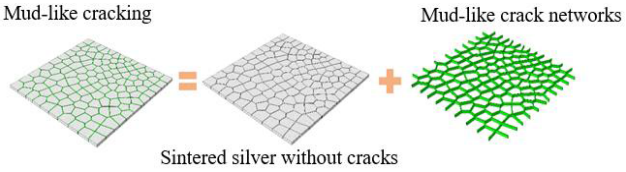

Fig. 6. Generated 3-D mud-cracking model in sintered Ag layer.

shown in Fig. 5 are presented. Based on the generated Voronoi polygons, here a position offset between the adjacent edges of polygons will be made. Note that the position offset produced here is the vertical cracking length. According to the experimental test of the mud-crack, the width of the crack in planar is around 9–50 μm, which depends on the detail cracking patterns [10], [23]. In this article, the length of the position offset among the adjacent edges of polygons is set as 10 μm [shown in Fig. 5(b) and (c)].

Based on the generation of planar Voronoi polygons and cracks, the 3-D model for mud-cracking is built by extending the planar Voronoi polygons containing cracks in the vertical direction (see Fig. 6). Then, a final 3-D mud-cracking model is generated, as shown in Fig. 6, where the model contains sintered Ag and the mud-cracks in sintered Ag.

After generating the 3-D mud-cracking model above in the commercial code MATLAB, all the nodes information about this model will be outputted and then import into the ABAQUS software as an input file via Python program to create the finite element model of the sintered Ag layer as well as the entire SiC power module.

B. Computational Framework

1) Equivalent Thermal Conductivity Computation of Sintered Ag Containing Mud-Cracks: The heat generated by the chips in the SiC package module is dissipated into the space in various ways. However, most of the heat flow is conducted vertically downward, and the heat transfer equation can be described by the 1-D Fourier law

$$q = -kA\frac{dT}{dx} = -kA\frac{\Delta T}{L} \tag{1}$$

where q, k, ΔT, A, and L are the heat flux, thermal conductivity, temperature discrepancy, effective heat transfer area, and length of the thermal conduction, respectively. For the porous sintered Ag containing cracks, the equivalent thermal conductivity of sintered Ag is given as follows:

$$k_{\text{eq}} = -\frac{q_z L_3}{\Delta T} = -\frac{\left(\sum_{i=1}^{n} q_z^i + \sum_{j=1}^{m} q_{z\text{crack}}^j\right) L_3}{T_u - T_l} \tag{2}$$

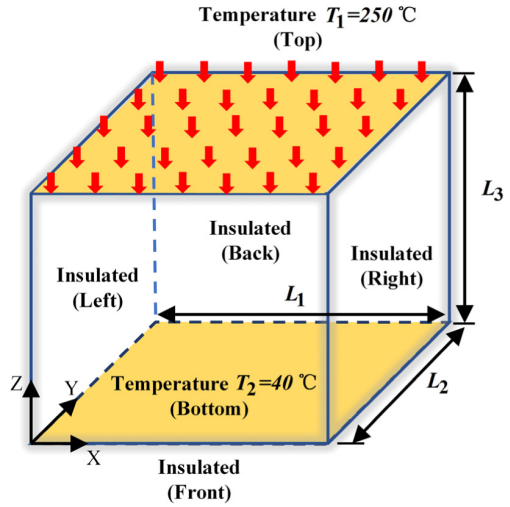

Fig. 7. Computation scheme of equivalent thermal conductivity of sintered silver layer considering mud-cracks.

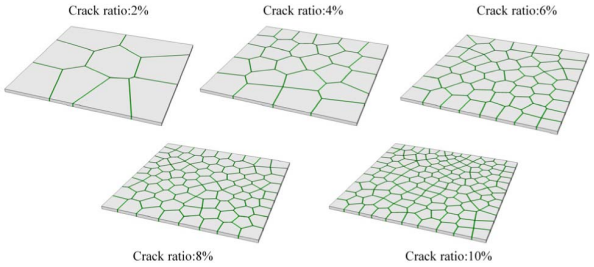

Fig. 8. Finite element model of sintered Ag with different crack ratios.

in which k_{eq} and L_3 are the equivalent thermal conductivity and length of thermal conduction path, respectively. T_u and T_l are the temperatures at the upper and lower bounds, as shown in Fig. 7. q_z^i and $q_{z\text{crack}}^j$ are the discrete heat flux of the ith element of sintered Ag and the jth element of the mud-cracks at a specific section perpendicular to the direction of heat flow, respectively.

Fig. 8 shows the finite element model of the sintered Ag with different crack ratios. The effect of crack ratios and porosities on the equivalent thermal conductivity of sintered Ag layer is studied according to the established models. Based on our previous computational scheme for equivalent thermal conductivity of sintered Ag containing cracks [16], [17], the equivalent thermal conductivity of the sintered Ag with mud-cracking can also be obtained by extracting the heat flux under 3-D conditions.

2) Power Cycling Simulation: In the present industrial condition, SiC devices are only partially used in MOSFET devices, and SiC-based insulated gate bipolar translator (IGBT) devices have not been commercialized. As a compromise, the geometry parameters of the SiC virtual module in this article refer to the BOG450H12E2AA half-bridge IGBT module [24] to perform the numerical analysis, as shown in Fig. 10. The detail geometry of the computed model has been listed in Table I. The material parameters adopted in this article are listed in Table II. Fig. 9 shows the detail

TABLE II
MATERIAL PARAMETERS USED IN THE SIMULATION

Material	Heat conductivity (W/(m·K))	Heat capacity (J/(kg·K))	Density(kg/m3)
SiC	170	670	3210
Sintered silver	porosity dependent	234	porosity dependent
Crack	0.026	1000	1.3
Copper	390	390	8960
AlN	160	740	3780
TIM (SAC305)	64	234	7400

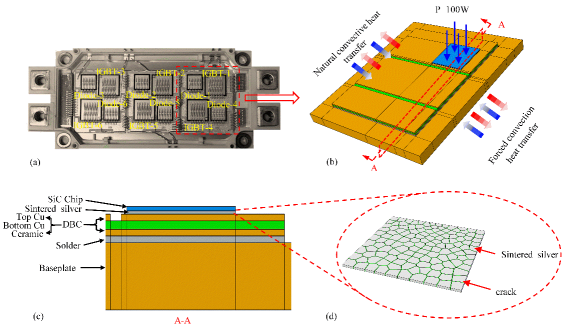

Fig. 9. Configuration of adopted SiC module. (a) Real Si-IGBT module. (b) Single module. (c) Schematic of each layer structure along the A–A section. (d) Enlarged view of sintered Ag layer.

finite element model and boundary conditions for the power cycling simulation. In the finite element model, eight nodes heat transfer brick element (DC3D8) is adopted. The power loss of the SiC chip when the device is switching ON is set as 100 W. The time for the chip switching ON and switching OFF is set as 2 s/2 s to simulate the power cycling condition. An equivalent convection coefficient of 3000 W/(m^2·K) is applied on the bottom of the Cu baseplate to simulate the liquid cooling, whereas the other surfaces are applied a convection coefficient 10 W/(m^2·K) considering the natural convection heat transfer. In addition, the ambient temperature is set as 25 °C.

To study the effect of geometry parameters on the heat transfer behavior of the SiC power module, four different chip sizes and sintered Ag thicknesses, as listed in Table I, are adopted. In addition, the effect of the mud-cracking density and porosity of the sintered Ag layer on the transfer behaviors of the power module are also considered. To quantitatively characterize the heat transfer behavior of the power module, the thermal resistance of the SiC power module is calculated for each condition. The definition of the thermal resistance can be expressed as

$$R_{\text{th}} = \frac{T_j - T_c}{P} \tag{3}$$

where T_j is the junction temperature of the SiC chip, T_c is the temperature of the baseplate, and P is the power loss of the SiC chip, respectively.

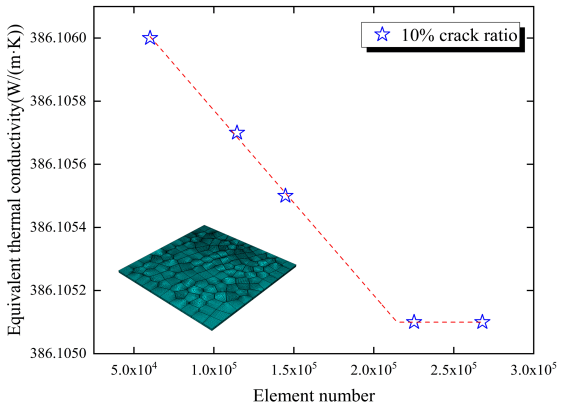

Fig. 10. Meshing of the sintered Ag layer and variation of the equivalent thermal conductivity with the element number.

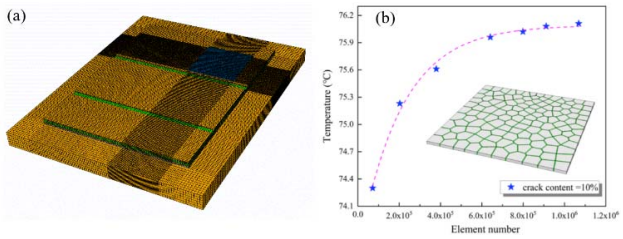

Fig. 11. Convergence validation of the finite element model. (a) Meshing grid of the SiC power module. (b) Variation of the calculated maximum junction temperature with the element number.

IV. Results

A. Convergence Analysis of the Finite Element Model

In order to obtain a convergent and accurate solution during the simulation, the validation of the finite element model is presented. Fig. 10 shows the meshing of the sintered Ag layer and variation of the equivalent thermal conductivity with the element number. It is seen that the equivalent thermal conductivity will converge when the number of the elements exceeds 220 000. Fig. 11 shows the meshing of the SiC power module and variation of the junction temperature with the element number. It is seen that the junction temperature will converge when the total number of elements exceeds 700 000. Hence, in the following studies, for the equivalent thermal conductivity calculation and the power cycling simulation, the element numbers are all exceed 220 000 and 700 000 to ensure the convergence.

B. Mud-Cracking Effect on Equivalent Thermal Conductivity of Sintered Silver

Fig. 12 shows the variations of the equivalent thermal conductivity of sintered Ag with different crack ratios at a porosity of 5%. It is seen clearly that the equivalent thermal conductivity of sintered Ag approximately decreases with increase of crack ratio linearly. When the crack ratio is 10%, the equivalent thermal conductivity decreases by about 8%. In addition, the equivalent thermal conductivity of sintered Ag also decreases linearly with the increase of porosity of sintered Ag, as shown in Fig. 13. In fact, Hoenig [25] proposed a formula to predict the effective thermal conductivity of

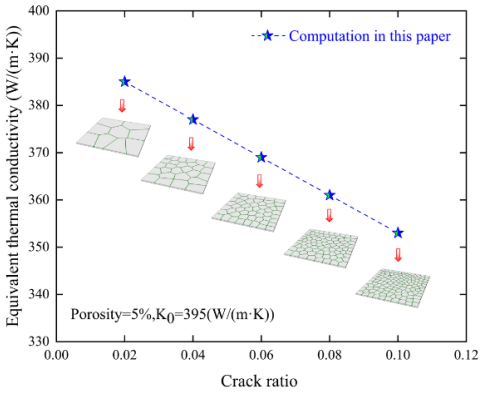

Fig. 12. Variations of the equivalent thermal conductivity of sintered Ag with different crack ratios at a porosity of 5%.

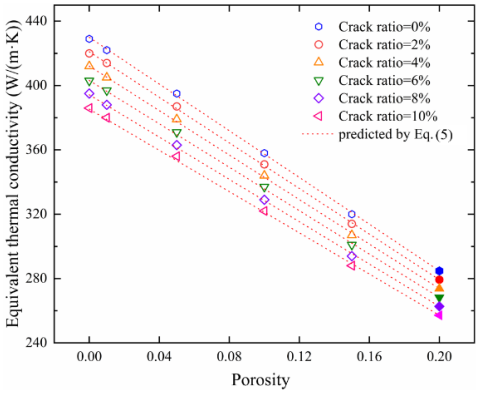

Fig. 13. Effect of porosity and crack ratio on the equivalent thermal conductivity of sintered Ag.

a solid with flat elliptical cracks where the form is written as follows:

$$K_{\mathrm{eq}} = K_0\left(1 - \frac{8}{9}\varphi\right) \tag{4}$$

where K_0 is the thermal conductivity without cracks, K_{eq} is the equivalent thermal conductivity, and φ is the crack ratio. Equation (4) is based on the assumptions that cracks are randomly distributed throughout the solid. The prediction formula shows that the effective thermal conductivity decreases as the crack ratio increases. However, the limitation of (4) is that it is applicable only under low crack ratio.

In order to overcome the shortage of (4), a following form is presented according to the regression analysis based on the numerical computation results in Fig. 13:

$$K_{\mathrm{eq}} = 429.94 - 725.76\varphi_{\mathrm{p}} - 446.32\varphi_c + 852.29\varphi_c\varphi_{\mathrm{p}} \tag{5}$$

where φ_c and φ_{p} are the porosity and crack ratio of sintered Ag layer, respectively. It is seen that the regression equation is good consistent with the numerical calculation results according to Fig. 13.

C. Temperature Distribution of the Module Under Power Cycling

Fig. 14 shows the temperature distribution of the power module without crack and with 10% mud-cracking ratio at

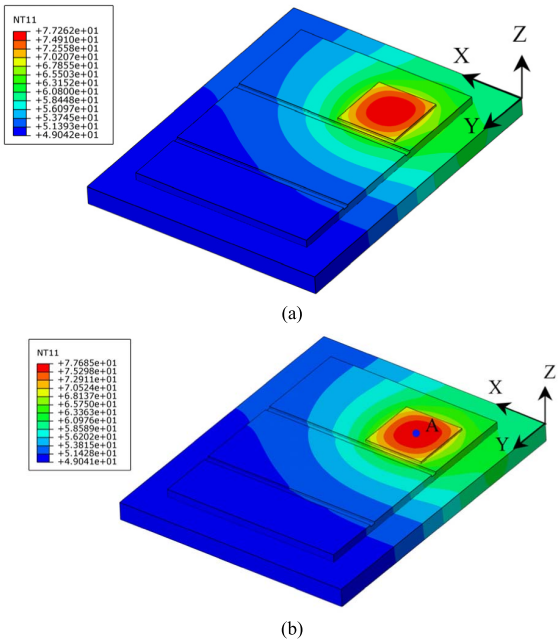

Fig. 14. Temperature distribution of the power module at the moment of power-OFF after five power cycles: (a) no crack and (b) with 10% crack ratio.

the moment of power-OFF after five power cycles, respectively. It is seen that the junction temperature for the module with 10% mud-crack is a little higher than that without any cracks. The reason for that is the existence of the mud-cracking lead to the degradation of the heat transfer characterization of the SiC power module.

Fig. 15 shows the variation of the junction temperature of the power module with 10% mud-cracking ratio with power cycling time. The junction temperature of the power module fluctuates repeatedly with the switching of the SiC device. The maximum junction temperature difference appears at the first power cycles and gradually decreases with the increase of the power cycles. After three power cycles, the junction temperature difference tends to be a stable value. Fig. 16 shows the temperature distribution for each packaging layer of the power module with 10% mud-crack ratio in the vertical direction at the moment of power-OFF after five power cycles. The temperature for each packaging layer is quite different. From the SiC chip to the copper baseplate, the temperature gradually decreases layer by layer.

V. Discussion

A. Effect of Mud-Crack Ratio on Thermal Resistance

Fig. 17 shows the effect of the mud-cracking ratio on the thermal resistance of the power module. The results show that the thermal resistance of the power module also increases linearly with the increase of the crack ratio. When the mud-crack ratio increases by 10%, the thermal resistance of the power module increases by about 0.12%. The increase of the thermal resistance will lead to the further increase of the maximum junction temperature difference, which will accelerate the damage of the sintered Ag layer, and lead to the failure of the entire power module.

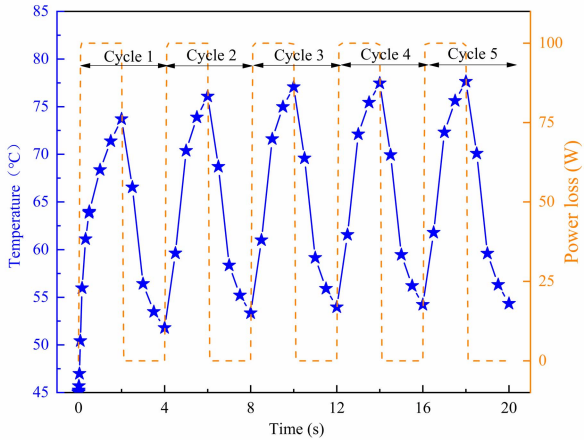

Fig. 15. Variation of the junction temperature of the power module with power cycling time.

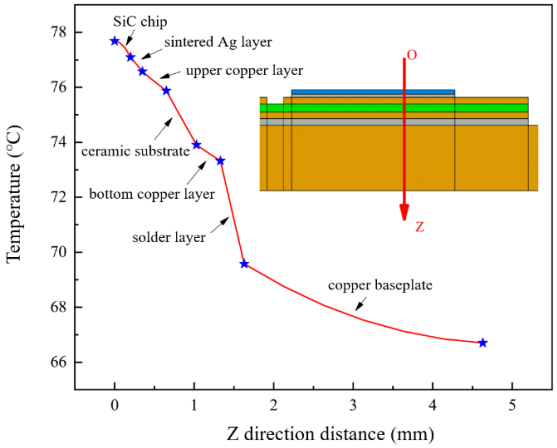

Fig. 16. Temperature distribution for each packaging layer in the vertical direction.

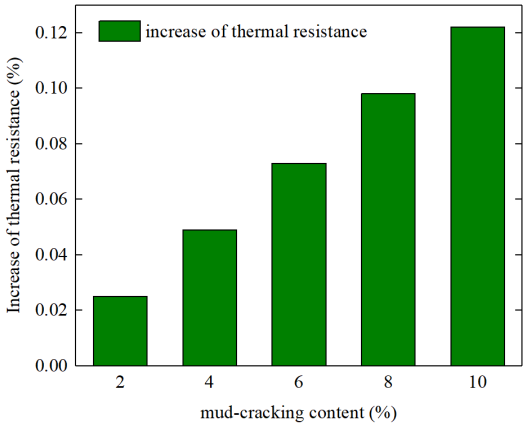

Fig. 17. Effect of the mud-cracking ratio on the thermal resistance of the SiC power module.

B. Effect of Chip Size, Thickness, and Porosity of Sintered Ag on Thermal Resistance

Fig. 18 shows the effect of sintered Ag thickness and porosity on the thermal resistance of the SiC power module with different chip sizes. It is found that the thermal

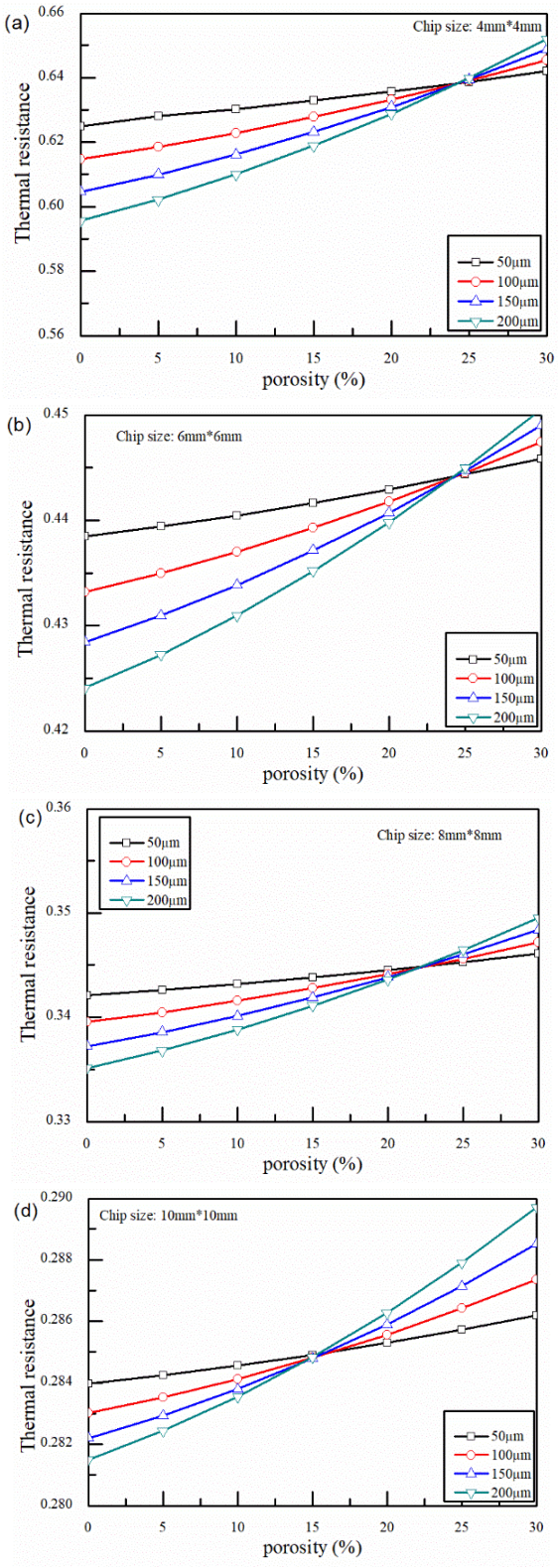

Fig. 18. Effect of sintered Ag thickness and porosity on the thermal resistance of the module with different chip sizes: (a) chip size with 4 mm × 4 mm; (b) chip size with 6 mm × 6 mm; (c) chip size with 8 mm × 8 mm; and (d) chip size with 10 mm × 10 mm.

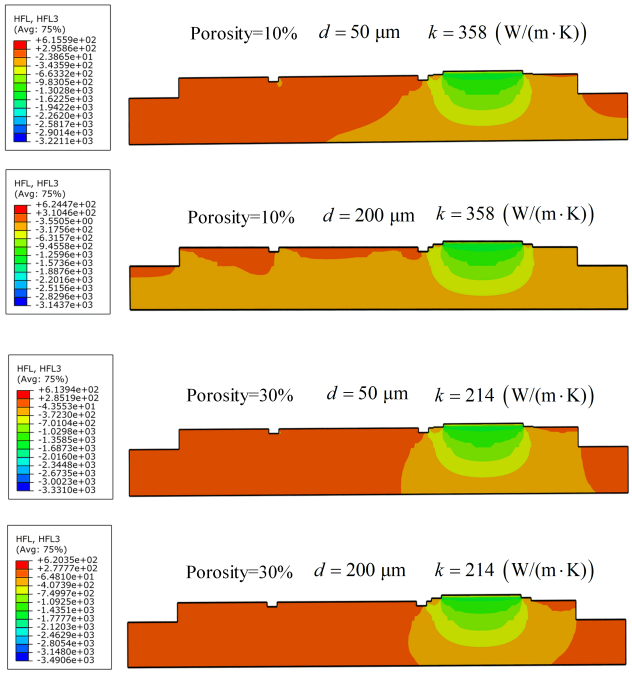

Fig. 19. Heat flux profiles for the power modules with different porosities and sintered Ag thicknesses.

resistance of the power module increases almost linearly with the increase of porosity. The reason is that the increase of the porosity will linearly decrease the thermal conductivity of the sintered Ag layer. Moreover, the growing slope of the thermal resistance versus the porosity increases with the increase of the sintered Ag thickness. The reason is that the thermal resistance of the sintered Ag layer is larger when the sintered Ag layer is thicker. Hence, the contribution of the sintered Ag on the thermal resistance of the entire power module will also increase with the increase of sintered Ag thickness. This is the reason that the thermal resistance of the power module with thicker sintered Ag layer more sensitive with the change of porosity. When the porosity and thickness of sintered Ag are confirmed, the thermal resistance will decrease with the increase of the chip size. It is not difficult to understand that a large chip size will increase the heat transfer area in the vertical direction, which is benefit for the heat dissipation of the SiC power module.

In addition, it is seen that the thermal resistance of the module decreases with the increase of the thickness of sintered Ag when the porosity is under a threshold value. However, when the porosity exceeds the threshold value, the thermal resistance of the module increases with the increase of the thickness of sintered Ag.

In order to further study the causes of the porosity threshold, the distribution of the heat flux across the Z–Y cross section for the power module is also extracted. Fig. 19 shows the heat flux profile for the power modules with porosities of 10%, 30%, and sintered Ag thickness of 50 and 200 μm, respectively. When the porosity is lower than the threshold value, the heat flux distribution becomes more homogenous with the increase of the sintered Ag thickness. However, when the porosity is higher than the threshold value, the heat flux distribution tends to be more uneven with the increase of the sintered Ag thickness. The reason is that, on the one hand,

TABLE III
COMPARISON OF THE COMPUTATIONAL SOLUTIONS BETWEEN MUD-CRACK MODEL AND EQUIVALENT MODEL

Method modeling	Number of elements	$T_{\text{j-max}}$ (°C)	R_{th} (°C/W)	Computational time (h)
Mud-crack model	779,508	77.679	0.28639	1
Equivalent model	745,374	77.675	0.28635	1/3

the increase of the sintered Ag thickness will increase the thermal resistance of the sintered Ag layer. This will increase uneven distribution of the heat flux as well as the thermal resistance of the entire power module when the porosity is higher than the threshold value. On the other hand, due to the exist of thermal transfer angle, the increase of the sintered Ag thickness will increase the effective thermal conduction area under the sintered Ag layer, which will decrease the thermal resistance of the direct bonded copper (DBC) substrate and the Cu baseplate. This will increase the homogenous of the heat flux distribution and decrease the thermal resistance of the entire power module when the porosity is lower than the threshold value.

C. On the Equivalent Model

Although the proposed mud-cracking model can provide an accurate estimation of the heat transfer behaviors of the sintered Ag layer, the computation cost is relatively increased. To increase the calculation efficiency, an equivalent model is developed based on replacing the mud-cracking model of sintered Ag with the equivalent bulk model. The thermal conductivity of the sintered Ag layer in the equivalent model is calculated according to (5). This equivalent method can also refer to [16] and [17]. The comparison of the equivalent model and the mud-cracking model is listed in Table III where the maximum temperature, thermal resistance, and computational time are given. It is found that the thermal resistance as well as maximum temperature for these two models are very close to each other. However, the computational time is only 1 h/3 h compared with that of the mud-crack model, which has been greatly decreased.

VI. CONCLUSION

This article presents a Voronoi tessellation model to quantitively study the effect of mud-cracking of sintered Ag layer on the heat transfer behaviors of SiC power module under power cycling conditions. The main conclusions are summarized as follows.

1) The proposed Voronoi tessellation model is verified to be reasonable to study the mud-cracking effect on the equivalent thermal conductivity of sintered silver layer as well as the heat transfer behaviors of the power module.
2) Effects of different crack ratio on the equivalent thermal conductivity of sintered Ag layer based on the mud-cracking model are studied. The equivalent thermal conductivity of the sintered Ag layer gradually decreases with the increases of crack ratio. An empirical model is proposed to describe the equivalent thermal conductivity of sintered Ag containing mud-cracks. Temperature distributions of the SiC power module with and without mud-cracks under power cycling conditions are also studied.
3) The effect of crack ratio, chip size, sintered Ag thickness, and porosity on the thermal resistance of the entire power module is analyzed. The thermal resistance of the power module increases almost linearly with the increase of the crack ratio and porosity, while decreases with the increase of the chip size. As for the effect of sintered Ag thickness, when the porosity is lower than the threshold value, the thermal resistance decreases with the increase of the sintered Ag thickness. When the porosity is higher than the threshold value, the thermal resistance increases with the increase of the sintered Ag thickness.
4) An equivalent model is also proposed and is proven to be accurate and efficient to study the effect of the mud-cracking of sintered Ag layer on the heat transfer behaviors of SiC power module under power cycling conditions.

REFERENCES

[1] T. F. Chen and K. S. Siow, "Comparing the mechanical and thermal-electrical properties of sintered copper (Cu) and sintered silver (Ag) joints," *J. Alloys Compounds*, vol. 866, Jun. 2021, Art. no. 158783.
[2] K. S. Siow, "Are sintered silver joints ready for use as interconnect material in microelectronic packaging?" *J. Electron. Mater.*, vol. 43, no. 4, pp. 947–961, Jan. 2014.
[3] C. Ding, H. Liu, K. D. T. Ngo, R. Burgos, and G.-Q. Lu, "A double-side cooled SiC MOSFET power module with sintered-silver interposers: I-design, simulation, fabrication, and performance characterization," *IEEE Trans. Power Electron.*, vol. 36, no. 10, pp. 11672–11680, Oct. 2021.
[4] R. Kimura, Y. Kariya, N. Mizumura, and K. Sasaki, "Effect of sintering temperature on fatigue crack propagation rate of sintered ag nanoparticles," *Mater. Trans.*, vol. 59, no. 4, pp. 612–619, 2018.
[5] Y. Tan, X. Li, G. Chen, Y. Mei, and X. Chen, "Three-dimensional visualization of the crack-growth behavior of nano-silver joints during shear creep," *J. Electron. Mater.*, vol. 44, no. 2, pp. 761–769, Feb. 2015.
[6] M. Hutter, C. Weber, C. Ehrhardt, and K. D. Lang, "Comparison of different technologies for the die attach of power semiconductor devices conducting active power cycling," in *Proc. 9th Int. Conf. Integr. Power Electron. Syst. (CIPS)*, Mar. 2016, pp. 1–7.
[7] N. Heuck *et al.*, "Aging of new interconnect-technologies of power-modules during power-cycling," in *Proc. 8th Int. Conf. Integr. Power Electron. Syst. (CIPS)*, Feb. 2014, pp. 1–6.
[8] T. Herboth, M. Guenther, A. Fix, and J. Wilde, "Failure mechanisms of sintered silver interconnections for power electronic applications," in *Proc. IEEE 63rd Electron. Compon. Technol. Conf.*, May 2013, pp. 1621–1627.
[9] J. Dai, J. Li, P. Agyakwa, and C. M. Johnson, "Power cycling reliability of time-reduced sintering for attaching SiC diodes using nanosilver film," in *Proc. 10th Int. Conf. Integr. Power Electron. Syst. (CIPS)*, Mar. 2018, pp. 1–6.
[10] J. R. Dai, J. F. Li, P. Agyakwa, M. Corfield, and C. M. Johnso, "Comparative thermal and structural characterization of sintered nano-silver and high-lead solder die attachments during power cycling," *IEEE Trans. Device Mater. Rel.*, vol. 18, no. 2, pp. 256–265, Jun. 2018.
[11] P. Agyakwa *et al.*, "Three-dimensional damage morphologies of thermomechanically deformed sintered nanosilver die attachments for power electronics modules," *J. Microsc.*, vol. 277, no. 3, pp. 140–153, Mar. 2020.
[12] T. Youssef *et al.*, "Power modules die attach: A comprehensive evolution of the nanosilver sintering physical properties versus its porosity," *Microelectron. Rel.*, vol. 55, pp. 1997–2002, Aug./Sep. 2015.
[13] A. A. Wereszczak, D. J. Vuono, H. Wang, M. K. Ferber, and Z. Liang, "Poperties of bulk sintered silver as a function of porosity," Oak Ridge Nat. Lab. (ORNL), Oak Ridge, TN, USA, Tech. Rep. ORNL/TM-2012/130, Jun. 2012.

[14] C. J. Hyun, R. Kyongtae, P. Kyunghoon, and S.-J. Moon, "Thermal conductivity estimation of inkjet-printed silver nanoparticle ink during continuous wave laser sintering," *Int. J. Heat Mass Transf.*, vol. 85, pp. 904–909, Jun. 2015.
[15] L. Signor *et al.*, "Evolution of the thermal conductivity of sintered silver joints with their porosity predicted by the finite element analysis of real 3D microstructures," *J. Electron. Mater.*, vol. 47, no. 7, pp. 4170–4176, Mar. 2018.
[16] F. Qin, Y. Hu, Y. Dai, P. Chen, and T. An, "Evaluation of thermal conductivity for sintered silver considering aging effect with microstructure based model," *Microelectron. Reliab.*, vol. 108, May 2015, Art. no. 112633.
[17] F. Qin *et al.*, "Crack effect on the equivalent thermal conductivity of porously sintered silver," *J. Electron. Mater.*, vol. 49, no. 10, pp. 5994–6008, Oct. 2020.
[18] Y. Wang, H. Liu, X. Ling, and Y. Weng, "Effects of pore microstructure on the effective thermal conductivity of thermal barrier coatings," *Appl. Thermal Eng.*, vol. 102, pp. 234–242, Jun. 2016.
[19] J. Chen, M. Zhang, H. Wang, and L. Li, "Evaluation of thermal conductivity of asphalt concrete with heterogeneous microstructure," *Appl. Thermal Eng.*, vol. 84, pp. 368–374, Jun. 2015.
[20] N. Selvakumar, M. Sivaraj, and S. Muthuraman, "Microstructure characterization and thermal properties of al-TiC sintered nano composites," *Appl. Thermal Eng.*, vol. 107, pp. 625–632, Aug. 2016.
[21] I. Sumirat, Y. Ando, and S. Shimamura, "Theoretical consideration of the effect of porosity on thermal conductivity of porous materials," *J. Porous Mater.*, vol. 13, nos. 3–4, pp. 439–443, Aug. 2006.
[22] A. EI Moumen, T. Kanit, A. Imad, and H. EI Minor, "Computational thermal conductivity in porous materials using homogenization techniques," *Comput. Mater. Sci.*, vol. 97, pp. 148–158, Feb. 2015.
[23] I. L. Regalado, J. J. Williams, S. Joshi, E. M. Dede, Y. Liu, and N. Chawla, "X-ray microtomography of thermal cycling damage in sintered nano-silver solder joints," *Adv. Eng. Mater.*, vol. 21, no. 3, Jan. 2019, Art. no. 1801029.
[24] J. Zhao *et al.*, "A study on the effect of microstructure evolution of the aluminum metallization layer on its electrical performance during power cycling," *IEEE Trans. Power Electron.*, vol. 34, no. 11, pp. 11036–11045, Nov. 2019.
[25] A. Hoenig, "Thermal conductivities of a cracked solid," *J. Compos. Mater.*, vol. 17, no. 3, pp. 231–237, May 1983.

Fei Qin received the B.E. degree in applied mechanics from Xi'an Jiaotong University, Xi'an, China, in 1985, and the M.E. and Ph.D. degrees in solid mechanics from Tsinghua University, Beijing, China, in 1987 and 1997, respectively.

He was a Post-Doctoral Fellow and a Research Fellow with the School of Civil and Structures, Nanyang Technological University, Singapore, from 1997 to 2000. He has been with Beijing University of Technology, Beijing, since 2001, where he is currently a Full Professor and the Director of the Institute of Electronics Packaging Technology and Reliability. He has authored or coauthored more than 150 journal articles and conference papers. He holds two U.S. patents and more than 50 Chinese patents. His current research interests include the areas of computer methods in materials science and engineering, design for reliability of electronic packaging, simulations, and characterization of the mechanical behavior of the materials, and structures and manufacturing processes in electronic packages.

Shuai Zhao received the B.E. degree in mechanical engineering from North China Electronic Power University, Baoding, China, in 2014. He is currently pursuing the Ph.D. degree in mechanics with Beijing University of Technology, Beijing, China.

His current research interests include reliability of materials and structure in the field of electronic packaging, including the thermal and mechanical modeling, packaging reliability, 3-D integration technology, and mechanical characterization of packaging materials.

Yanwei Dai received the B.E. degree in engineering mechanics from Wuhan University of Technology, Wuhan, China, in 2011, the M.E. degree in solids mechanics from China Agricultural University, Beijing, China, in 2013, and the Ph.D. degree in mechanics from Tsinghua University, Beijing, China, in 2018.

He has been an Associate Professor with the Institute of Electronics Packaging Technology and Reliability, Beijing University of Technology, Beijing, since 2020. He has authored or coauthored more than 40 SCI-indexed journal articles. He has been a Principal Investigator of more than ten projects which were granted by NSFC, BJNSF, or enterprises. His current research interests include the areas of fracture mechanics at elevated temperature in materials science and engineering as well as reliability evaluation and mechanical behavior characterization of the materials and structures in electronic packaging.

Yuankun Hu received the B.E. degree in mechanism design and automatization from the Hunan Institute of Engineering, Xiangtan, China, in 2018, and the M.E. degree in mechanics from Beijing University of Technology, Beijing, China, in 2021.

He is currently a Reliability Engineer with the Gree Group (China), Zhuhai, China. His current research interests include reliability of electronic packaging and microelectronics failure analysis.

Tong An received the B.E. degree in safety engineering, the M.E. degree in solids mechanics, and the Ph.D. degree in engineering mechanics from Beijing University of Technology, Beijing, China, in 2006, 2009, and 2014, respectively.

She was a Visiting Fellow with the Department of Electrical and Electronic Engineering, University of Nottingham, Nottingham, U.K., from 2019 to 2020. She is currently an Associate Professor with the Institute of Electronics Packaging Technology and Reliability, Beijing University of Technology. Her current research interests include reliability of power semiconductor device, thermomechanical modeling, failure mechanism of electronic packaging, and micro- and macro-mechanical behaviors of packaging materials.

Yanpeng Gong received the Ph.D. degree from the Department of Mechanics, School of Astronautics, Beijing Institute of Technology, Beijing, China, in 2019.

He was with the Department of Engineering, Durham University, Durham, U.K., from 2017 to 2018. He has been a Lecturer with the Institute of Electronics Packaging Technology and Reliability, Beijing University of Technology, Beijing, since 2019. His current research interests include new computer methods in materials science and engineering, heat conduction and thermal–mechanical modeling, and reliability of electronic packaging.